THE JOURNAL OF BIOLOGICAL CHEMISTRY
Vol. 275, No. 17, Issue of April 28, pp. 12400–12409, 2000
Printed in U.S.A.

Site-directed Mutagenesis of 2,4-Dichlorophenoxyacetic Acid/α-Ketoglutarate Dioxygenase

IDENTIFICATION OF RESIDUES INVOLVED IN METALLOCENTER FORMATION AND SUBSTRATE BINDING*

(Received for publication, January 18, 2000)

Deborah A. Hogan‡§¶, Sheila R. Smith‖, Eric A. Saari‖, John McCracken‖, and Robert P. Hausinger‡§‡‡**

*From the ‡Center for Microbial Ecology and Departments of §Microbiology, ‖Chemistry, and **Biochemistry, Michigan State University, East Lansing, Michigan 48824*

2,4-Dichlorophenoxyacetic acid (2,4-D)/α-ketoglutarate (α-KG) dioxygenase (TfdA) is an Fe(II)-dependent enzyme that catalyzes the first step in degradation of the herbicide 2,4-D. The active site structures of a small number of enzymes within the α-KG-dependent dioxygenase superfamily have been characterized and shown to have a similar HXDX$_{50-70}$HX$_{10}$RXS arrangement of residues that make up the binding sites for Fe(II) and α-KG. TfdA does not have obvious homology to the dioxygenases containing the above motif but is related in sequence to eight other enzymes in the superfamily that form a distinct consensus sequence (HX(D/E)X$_{138-207}$HX$_{10}$R/K). Variants of TfdA were created to examine the roles of putative metal-binding residues and the functions of the other seven histidines in this protein. The H167A, H200A, H213A, H245A, and H262A forms of TfdA formed inclusion bodies when overproduced in *Escherichia coli* DH5α; however, these proteins were soluble when fused to the maltose-binding protein (MBP). MBP-TfdA exhibited kinetic parameters similar to the native enzyme. The H8A and H235A variants were catalytically similar to wild-type TfdA. MBP-H213A and H216A TfdA have elevated K_m values for 2,4-D, and the former showed a decreased k_{cat}, suggesting these residues may affect substrate binding or catalysis. The H113A, D115A, MBP-H167A, MBP-H200A, MBP-H245A and MBP-H262A variants of TfdA were inactive. Gel filtration analysis revealed that the latter two proteins were highly aggregated. The remaining four inactive variants were examined in their Cu(II)-substituted forms by EPR and electron spin-echo envelope modulation (ESEEM) spectroscopic methods. Changes in EPR spectra upon addition of substrates indicated that copper was present at the active site in the H113A and D115A variants. ESEEM analysis revealed that two histidines are bound equatorially to the copper in the D115A and MBP-H167A TfdA variants. The experimental data and sequence analysis lead us to conclude that His-113, Asp-115, and His-262 are likely metal ligands in TfdA and that His-213 may aid in catalysis or binding of 2,4-D.

2,4-Dichlorophenoxyacetic acid (2,4-D)[1]/α-ketoglutarate (α-KG) dioxygenase (TfdA) is an Fe(II)- and α-KG-dependent enzyme that catalyzes the first step in degradation of the herbicide 2,4-D. This enzyme couples the oxidative decarboxylation of α-KG to the hydroxylation of a side chain carbon atom. The resultant hemiacetal spontaneously decomposes to form 2,4-dichlorophenol and glyoxalate (1). Mechanistically, TfdA resembles numerous other α-KG-dependent dioxygenases from plants, animals, fungi, and bacteria that catalyze similar hydroxylation reactions at unactivated carbon centers (2, 3).

Members of the α-KG-dependent dioxygenase superfamily are not closely related by their sequences but rather appear to fall into one of three groups of related enzymes or fall into a fourth group of unrelated sequences (4). The best studied α-KG-dependent hydroxylases, including prolyl and lysyl hydroxylase (5) and flavanone hydroxylase (3, 6), have an HXDX$_{\sim 55}$HX$_{10}$RXS motif in common (7, 8), and this motif is present in the more than 20 enzymes, defined here as Group I, within the α-KG dependent dioxygenase superfamily (8, 9). Site-directed mutagenesis studies have confirmed the importance of these residues for activity (8, 10–13), and the crystal structures of two Group I enzymes, isopenicillin *N* synthase (IPNS) and deacetoxycephalosporin C synthase (DAOCS), indicate that these residues comprise the metallocenter and α-KG-binding site (14–17). TfdA is not closely related in sequence to the Group I α-KG-dependent dioxygenases described above but is clearly homologous (25–30% identity) to *Escherichia coli* taurine/α-KG dioxygenase (TauD) (18) and sulfonate/α-KG dioxygenase from *Saccharomyces cerevisiae* (19). Furthermore, PSI-BLAST analyses (20) find additional rela-

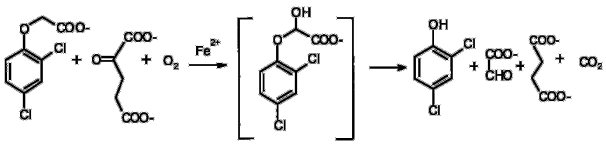

SCHEME 1

* This research was supported in part by National Science Foundation Grants DEB9120006 and MCB 9603520 (to R. P. H), National Institutes of Health Grant GM 54065 (to J. M.), and the Michigan State University Agricultural Experiment Station. The costs of publication of this article were defrayed in part by the payment of page charges. This article must therefore be hereby marked "*advertisement*" in accordance with 18 U.S.C. Section 1734 solely to indicate this fact.

¶ Supported in part by National Institutes of Health Biotechnology Training Grant T32-GM08350.

‡‡ To whom correspondence should be addressed: 160 Giltner Hall, Dept. of Microbiology, Michigan State University, East Lansing, MI 48824. Tel.: 517-353-9675; Fax.: 517-353-8957; E-mail: Hausinge@pilot.msu.edu.

[1] The abbreviations used are: 2,4-D, 2,4-dichlorophenoxyacetic acid; α-KG, α-ketoglutarate; TfdA, 2,4-D/α-KG dioxygenase; TauD, taurine/α-KG dioxygenase; cw-EPR, continuous wave electron paramagnetic resonance; ESEEM, electron spin echo envelope modulation; IPNS, isopenicillin *N* synthase; DAOCS, deacetoxycephalosporin synthase; MBP, maltose-binding protein; FT, Fourier transform; MOPS, 4-morpholinepropanesulfonic acid.

TABLE I
Consensus motifs for subgroups within the α-KG-dependent dioxygenase superfamily

Group I (IPNS, DAOCS, and related enzymes)	H*X*D	X_{50-70}	HX_{10}(R/K)*X*S
Group II (TfdA, TauD, clavaminate synthase and related enzymes)	H*X*(D/E)	$X_{138-207}$	HX_{10-13}R
Group III (Phytanoyl-CoA hydroxylase, proline hydroxylase and related enzymes)	H*X*D	X_{72-101}	HX_{10}(R/K)*X*S

tionships to γ-butyrobetaine hydroxylase and clavaminate synthase. Alignment of these Group II sequences indicates the conservation of two histidines and one aspartate (His-113, His-262, and Asp 115 in TfdA) as well as an invariant arginine that may be analogous to the α-KG-binding arginine in DAOCS and related enzymes (Table I). A third set of enzyme sequences (Group III) from members of the α-KG-dependent dioxygenase superfamily, including phytanoyl-CoA hydroxylase and proline hydroxylase, exhibit the presence of a third related motif despite the lack of overall sequence similarity to Group I or Group II enzymes.

In this study, we used site-directed mutagenesis methods to examine the roles of potential metal-binding residues in the above motif (His-113, His-262, and Asp-115) and the remaining seven histidines in TfdA. Previously published work showed that TfdA was inactivated by diethylpyrocarbonate, a histidine-selective reagent, and provided evidence consistent with the presence of multiple histidines in the active site (21). Spectroscopic studies of TfdA showed the presence of two equatorially bound imidazole nitrogens as ligands to the active site metal and indicated that one imidazole ligand may be displaced or shifted to an axial position upon substrate binding (22–24). Based on analyses of different TfdA variants, we identify several likely metal ligands and provide evidence that another one or two histidines may aid in substrate binding.

EXPERIMENTAL PROCEDURES

Recombinant Plasmids—All plasmids were constructed from pUS311 (21), a pUC19 derivative that contains the *Ralstonia eutropha* JMP134 *tfdA* gene (Fig. 1). The H8A, D115A, H213A, H216A, H235A, H245A, and H262A TfdA variants were created by direct mutation of *tfdA* in pUS311 by the Stratagene Quickchange System (Stratagene, La Jolla, CA). All mutagenic primers are listed in Table II. Two alternative approaches were used to construct the three remaining variants. Plasmids encoding H113A and H167A TfdA variants were created by CLONTECH mutagenesis of pXHtfdA, a pUC19 plasmid containing the 5′-*Xba*I-*Hin*dII fragment of the *tfdA* gene (Fig. 1). To create the complete gene containing the indicated mutations, the *Xba*I-*Hin*dII fragment was cloned into pHKtfdA, which contains the 3′ end of the *tfdA* gene. pHKtfdA was constructed in two steps. First, the 1.4-kilobase pair *Xba*I-*Sal*I fragment from pUS311, containing the complete *tfdA* gene, was cloned into pBC KS$^-$ (Stratagene) cut with *Xba*I and *Xho*I to create pBCtfdA. This step had the benefit of eliminating a *Hin*dII site that interfered with further cloning steps. The 727-base pair *Hin*dII-*Kpn*I fragment of pBCtfdA was subcloned into pBC KS$^-$ cut with the same enzymes to give pHKtfdA. Similarly, the gene encoding H200A TfdA was made by mutagenesis of pXXtfdA, a pUC19 plasmid containing the 5′-*Xba*I-*Xho*I fragment of *tfdA*. The altered *Xba*I-*Xho*I fragment was then inserted into pHKtfdA cut with *Xba*I and *Xho*I to give the complete H200A *tfdA* gene. The identity of all final constructs was confirmed by sequence analysis. To insert the genes encoding H167A and H262A variants of TfdA into a plasmid that would allow for isopropyl-1-thio-β-D-galactopyranoside-controlled expression, the *Xba*I-*Sal*I fragments from the corresponding plasmids described above were cloned into pET23a (Novagen) prepared with the same enzymes.

To create the maltose-binding protein (MBP)-TfdA fusion proteins, the wild-type *tfdA* gene was amplified from pUS311 with TfdA-MBPF and TfdA-MBPR primers (Table II) to create an *Xba*I site directly upstream of the GTG start codon of the *tfdA* gene and a *Hin*dIII

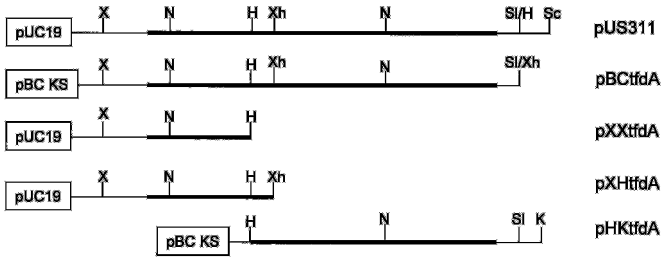

FIG. 1. **Restriction maps of the plasmids used in construction of *tfdA* mutants.** The abbreviations for the restriction enzyme sites are as follows: *H*, *Hin*dII; *X*, *Xba*I; *Xh*, *Xho*I; *Sl*, *Sal*I; *K*, *Kpn*I; *Sc*, *Sac*I; and *N*, *Nru*I. The vector backbone is indicated in the *box* on the *left*. The *tfdA* open reading frame is shown as a *wide*, *solid line*.

TABLE II
Sequences of mutagenic primers used to create altered tfdA genes

Mutant	Primer sequence[a]
H8A	5′-CGC AAA TCC CCT TGC TCC TCT TTT CGC C-3′
H113A	5′-GTC GCT GGC CCA AGC TGG-3′
D115A	5′-GCA CAG CGC CAG CTC CTT TCA-3′
H167A	5′-GCG TGC CGA GCA GTA CGC ACT G-3′
H200A	5′-GGT TCG AAC CGC CGC CGG CTC-3′
H213A	5′-GCT CGC GGC CGC GCC GAT-3′
H216A	5′-CCT TCG ACG GCG CTC GCG-3′
H235A	5′-GCT TCT CGA GGC GAC ACA G-3′
H245A	5′-GTG TAC CGG GCT CGC TGG AAC-3′
H262A	5′-CGT TCT TGC ACG CGG ACG CAG-3′
Tfda-MBPF	5′-TCT CTA GAG TGA GCG TCG TCG CAA ATC C-3′
Tfda-MBPR	5′-GTC AAG CTT GGT TGC GTA CAT CTT GTG G-3′

[a] The reverse primer used for the creation of all mutants was the complement of the forward primer.

WI). The *Xba*I-*Hin*dIII fragment was isolated from the resulting plasmid and cloned into the pMAL-c2 vector that had been digested with the same enzymes. The identity of the newly created *malE-tfdA* gene fusion was confirmed by sequencing. Substitution of the mutation-containing internal *Nru*I fragment for the same fragment of the wild-type *malE-tfdA* gene created MBP-fusion forms of altered TfdAs. First, pMAL-*tfdA* was digested with *Nru*I, and the vector fragment was purified and religated to create pMAL-*tfdA*Δ*Nru*I. The resultant plasmid was linearized with *Nru*I and dephosphorylated with calf intestine alkaline phosphatase prior to ligation with the *Nru*I fragments isolated from the previously described mutant genes. Constructs were confirmed by restriction analysis.

Protein Purification—H8A, H113A, D115A, H216A, H235A, and wild-type TfdA proteins were purified from *E. coli* DH5α cells carrying pUS311 and its mutated derivatives according to a previously described protocol (21). In addition, the non-mutated enzyme and the TfdA variants H167A, H200A, H213A, H245A, and H262A were purified as MBP-TfdA fusion proteins from *E. coli* DH5α by the protocol described in the pMAL Protein Fusion and Purification System Manual (New England Biolabs, Beverly, MA).

Analysis of Kinetic Parameters—Specific activities of the wild-type and variant TfdA proteins were determined by a previously described spectrophotometric assay (21). The typical assay mixture contained 1 mM 2,4-D, 1 mM α-KG, 100 μM $(NH_4)_2Fe(SO_4)_2$, and 100 μM ascorbic acid in 10 mM MOPS buffer (pH 6.75) at 30 °C. The reactions were quenched by the addition of EDTA to a concentration of 5 mM. 2,4-Dichlorophenol was quantified by reaction with 4-aminoantipyrene followed by meas-

the Bio-Rad Protein Assay with bovine serum albumin as a standard. For calculation of the k_{cat} values, the TfdA variants were assumed to have M_r = 31,600 and the MBP-TfdA variants were assigned M_r = 74,500.

The low K_m values for α-KG (~2–5 μM for the wild-type enzyme) precluded use of the 4-aminoantipyrene assay for accurate determination of this value. The alternative method used to measure the K_m values for α-KG quantified the amount of $^{14}CO_2$ liberated from α-[1-^{14}C]KG during the course of the reaction (21).

Native Protein Analysis by Gel Filtration—Size exclusion chromatography was used to estimate the native molecular weights of TfdA, MBP-TfdA, and mutant proteins. The proteins were chromatographed on a Superose 6 gel filtration column (1.0 × 30 cm, Amersham Pharmacia Biotech) in 20 mM Tris buffer (pH 7.5), 1 mM EDTA, and 200 mM NaCl at a flow rate of 0.2 ml·min^{-1}. The elution volumes were compared with those for gel filtration standards (Bio-Rad) including thyroglobulin, 670 kDa; bovine gamma globulin, 158 kDa; chicken ovalbumin, 44 kDa; myoglobin, 17 kDa; and vitamin B_{12}, 1350 Da.

Spectroscopic Analysis—Proteins for electron paramagnetic resonance (EPR) and electron spin-echo envelope modulation (ESEEM) spectroscopic analyses were exchanged into 25 mM MOPS (pH 6.75) by repeated concentration and dilution in Centricon 30 (Amicon) centrifugal concentrators. The final subunit concentration was 0.5 mM for the non-fusion forms of TfdA and 0.4 mM for the MBP-TfdA proteins. $CuCl_2$ was added to a concentration of 450 and 350 μM, respectively. Buffered solutions of α-KG and 2,4-D were added to final concentrations of 5 mM. Glycerol was present at 40% in all samples.

X-band EPR spectra were obtained at 77 K on a Bruker ESP-300E spectrometer. ESEEM data were collected on a home-built spectrometer; the microwave bridge of this instrument has been previously described in detail (25). Data collection and analyses were controlled by a Power Computing model 200 Power PC using software written with LabView version 5.01 (National Instruments). Electron spin echoes were digitized, averaged, and integrated by a Tektronix model 620B digital oscilloscope interfaced to the spectrometer computer via an IEEE-488 bus. Two four-channel delay and gate generators (Stanford Research Systems model DG535), a Bruker BH-15 magnetic field controller, and a Hewlett-Packard model 8656B radiofrequency synthesizer were also interfaced using IEEE-488 protocol. Data were collected using a reflection cavity that employed a folded microstrip resonator (26). A three-pulse stimulated echo sequence (90-τ-90°-T-90°) was used. ESEEM spectra were generated by Fourier transformation of the time domain data using dead time reconstruction (27). Simulations of the experimental data were performed on a Sun SparcII work station. Simulation programs were written in FORTRAN and based on the density matrix formalism developed by Mims (28). Software for the frequency analysis of the experimental and simulated data was written in Matlab (Mathworks, Natick, MA).

Sequence Comparisons—Related sequences were initially detected by BLAST (29) and PSI-BLAST (20) analyses. Alignments were generated with the CLUSTAL algorithm (30), and the figure was prepared using Genedoc (31).

RESULTS

Production of the Mutant TfdAs—Initially, all of the mutant genes were expressed from their pUC19-based plasmids except for those encoding H113A, H167A, and H200A TfdA, which were in pBC KS$^-$-derived plasmids. By using the standard protocol to produce soluble, wild-type TfdA (growth at 30 °C to early stationary phase), only the H8A, H113A, D115A, H216A, and H235A variants existed as soluble proteins. All of the other TfdA variants were present as inclusion bodies even when grown at lower temperatures (22 °C), in M9 minimal medium, or in LB broth containing 660 mM sorbitol and 2.5 mM betaine (32). In addition, isopropyl-1-thio-β-D-galactopyranoside-controlled production of H167A and H262A proteins from mutant genes cloned into pET23a did not yield soluble samples even when the harvested cell pellets were suspended in buffer containing 20% glycerol to limit protein aggregation.

To overcome the solubility problems for the five TfdA variants, MBP-TfdA fusion proteins were created. Wild-type TfdA metal binding capacity of MBP. Since the presence of the fusion protein did not appear to greatly affect the kinetic parameters of wild-type enzyme, similar fusion proteins were created for the H167A, H200A, H213A, H245A, and H262A TfdA variants.

TABLE III
Summary of the kinetic parameters for active TfdA variants

TfdA sample	k_{cat}	K_m αKG	K_m 2,4-D	K_D Fe(II)
	min^{-1}	μM	μM	μM
Wild type	442 ± 33	4.9 ± 0.73	19.3 ± 3.7	2.0 ± 0.5
MBP fusion	411 ± 23	9.9 ± 1.8	33.7 ± 2.5	15.2 ± 5.4
H8A[a]	284 ± 6.9	6.5 ± 1.8	17.7 ± 3.8	1.9 ± 0.7
MBP-H213A	22.1 ± 2.9	8.3 ± 2.9	318 ± 44	27.7 ± 9.8
H216A	474 ± 47	6.05 ± 2.6	52 ± 5	2.4 ± 1.7
H235A	284 ± 25	9.6 ± 1.6	34 ± 8	1.4 ± 1.7

[a] More than 75% of the protein was present as the degradation product. The k_{cat} was estimated from the active, full-length fraction.

Kinetic Analyses of Altered TfdAs—Results from kinetic analyses of the four active mutant proteins are summarized in Table III. H8A TfdA was soluble and active but was rapidly proteolyzed to an inactive form. By electrophoretic comparisons, the cleavage site appeared to be the same as in wild-type TfdA (between Arg-77 and Phe-78) (21). The rate of proteolysis of H8A TfdA was enhanced compared with that seen for the wild-type enzyme despite the presence of EDTA and protease inhibitors in the purification buffer. Because purified H8A TfdA was more than 75% degraded, the catalytic rate constant was calculated with the estimated amount of intact enzyme. These calculations indicate rates and K_m values similar to those for the wild-type enzyme. Similarly, the kinetic parameters for H235A TfdA were comparable to the native enzyme. In contrast, two variants exhibited differences from wild-type enzyme in their kinetic parameters. The H213A MBP-TfdA variant exhibited a 20-fold reduction in k_{cat} and a 10-fold increase in K_m for 2,4-D. In addition, H216A TfdA had a modest (2.5-fold) increase in the K_m for 2,4-D and no change in catalytic rate. The other kinetic parameters for H213A MBP-TfdA and H216A TfdA (K_m for α-KG and K_D for ferrous ion) did not differ significantly from the wild-type values. Six soluble TfdA variants (H113A, D115A, MBP-H167A, MBP-H200A, MBP-H245A, and MBP-H262A) exhibited no activity even when assayed with elevated substrate and cofactor concentrations (10 mM α-KG, 5 mM 2,4-D, and 250 μM Fe(II)).

Evaluation of the Structural Consequences of the Mutations—To assess whether the inactive mutant proteins assumed conformations similar to the wild-type enzyme, their apparent molecular weights were estimated by gel filtration analysis. The observed size of wild-type TfdA was found to be 51 kDa by comparison to protein standards, suggesting that TfdA forms a compact dimer or an elongated monomer. The elution volume for both H113A and D115A corresponded exactly to wild-type TfdA indicating that these proteins are not significantly altered in their quaternary structure. MBP-TfdA eluted both in the void volume (approximately 25% of the protein) and at a position corresponding to 216 kDa (roughly 75% of the protein), suggesting that MBP-TfdA forms at least a dimer. Because each MBP-TfdA subunit is comprised of two domains separated by a 13-amino acid linker, the resultant protein may migrate with a larger apparent molecular weight. MBP-H167A and MBP-H200A samples demonstrated the same two-peak profile as MBP-TfdA but with larger proportions eluting in the void volume. MBP-H245A and MBP-H262A proteins were soluble; however, gel filtration analysis indicated the presence of only highly aggregated material eluting in the void

EPR Spectroscopic Characterization of Variants with Altered Metal Sites—The metallocenter properties for selected TfdA variants were probed by EPR spectroscopy. To circumvent the problems that arise in EPR measurements of integer spin paramagnetic centers, Fe(II) was substituted with cupric ion. Although the Cu(II) form of TfdA is inactive, Cu(II) binds competitively with respect to Fe(II) (K_i = 1–3 μM), and copper-substituted TfdA has been used previously to study the metal coordination environment of this enzyme in the presence and absence of substrates (22–24). Spectral parameters of wild-type Cu(II)-TfdA, Cu(II)-TfdA + α-KG, and Cu(II)-TfdA + α-KG + 2,4-D (Fig. 2*A* and Table IV), agreed well with those reported previously (23, 24). Earlier studies of copper-substituted wild-type TfdA indicated that the metal is bound in a type 2 environment with a mixture of O and N ligands in the equatorial plane. Upon addition of α-KG and 2,4-D to the enzyme, the spectral parameters are altered to a more rhombic signal with accompanying resolution of ligand hyperfine coupling (Fig. 2*A*). These results suggest that binding of the co-substrates to the enzyme leads to a better defined copper site with α-KG binding directly to the metallocenter (23, 24). The small $A_{\|}$ (less than 14 mT) for the α-KG- and 2,4-D-bound sample indicates a significant distortion from planarity.

The four inactive mutant forms of TfdA with quaternary structures similar to the corresponding wild-type protein (H113A, D115A, MBP-H167A, and MBP-H200A) were analyzed by EPR spectroscopy to assess the metal coordination environments. No significant differences between the spectra of MBP-TfdA and the non-fusion wild-type TfdA were observed (data not shown). EPR spectra of the copper-substituted samples, in all cases, showed contributions from multiple copper sites indicating a mixture of copper centers, most likely resulting from copper binding in multiple conformations or at sites other than the active site. The presence of alternative copper-binding sites is not surprising in an enzyme with nine histidines.

The EPR spectra for Cu-H113A TfdA alone and in the presence of α-KG and 2,4-D (Fig. 2*B* and Table IV) differ significantly from spectra of wild-type enzyme and show modest changes in Cu(II) g values and hyperfine tensor principal values upon substrate additions. The broadening of the EPR signal in the $g_{\|}$ region upon addition of α-KG again suggests a mixture of copper site conformations. Thus, it appears that alteration of His-113 significantly affects the metal binding properties for TfdA such that copper is no longer constrained to a single active site configuration.

The EPR spectrum of D115A-TfdA (Fig. 2*C*) has parameters similar to those observed in the copper-substituted wild-type protein (Table IV), although with less resolution of $A_{\|}$. Addition of α-KG (in the presence or absence of 2,4-D) has a dramatic effect on the appearance of the D115A data, enhancing resolution of the Cu(II) hyperfine peaks at $g_{\|}$ and the ligand hyperfine structure in the $g_{\perp}$ region (Fig. 2*C*). The appearance of these superhyperfine interactions may result from a subtle shift in the orientation of the principal g tensor such that the imidazole ligands occupy an increasingly equatorial position (33). These results are consistent with the formation of a tighter or more regular copper-binding site upon addition of the co-substrate.

The EPR spectrum for MBP-H167A TfdA (Fig. 2*D*), like that for the H113A variant, is poorly resolved, probably due to binding of copper in multiple configurations instead of formation of one major conformation. Additionally, few significant changes are seen upon addition of either α-KG or 2,4-D. The MBP-H200A EPR spectrum (Fig. 2*E*) is better resolved than

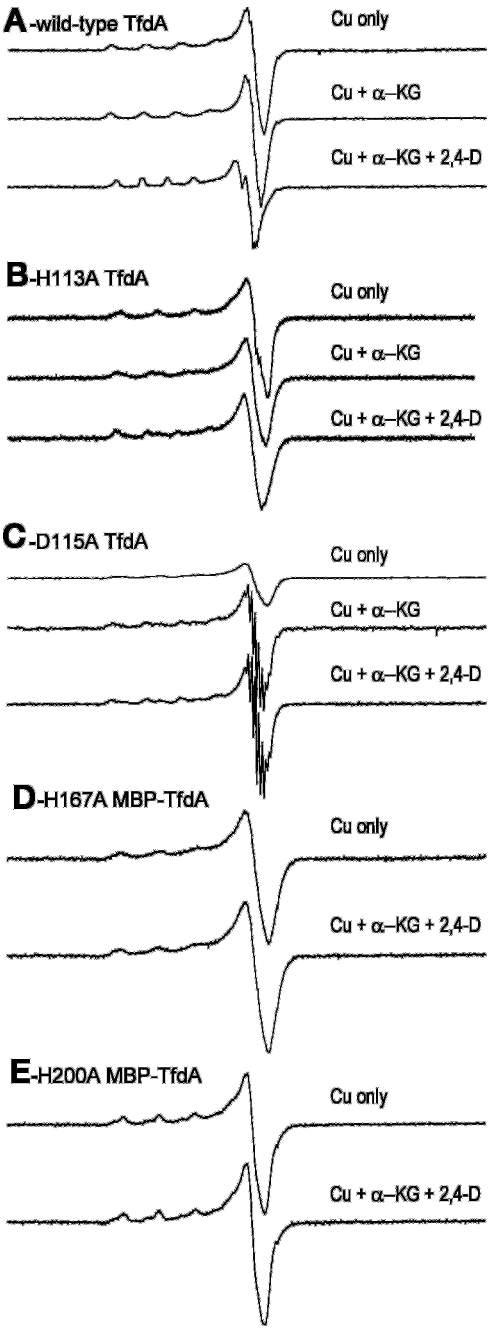

FIG. 2. **X-band CW-EPR spectra of Cu(II)-substituted TfdA variants.** EPR spectra were obtained at 77 K for the following samples (substrate concentrations were 5 mM, when present). *Top* to *bottom,* wild-type Cu-TfdA in the absence of substrates, with α-KG, and with α-KG + 2,4-D (*A*). H113A Cu-TfdA in the absence of substrates, with α-KG, and with α-KG + 2,4-D (*B*). D115A Cu-TfdA in the absence of substrates, with α-KG, and with α-KG + 2,4-D (*C*). MBP-H167A Cu-TfdA in the absence of substrates, with α-KG, and with α-KG + 2,4-D (*D*). MBP-H200A Cu-TfdA in the absence of substrates and in the presence of α-KG + 2,4-D (*E*). Spectral parameters are listed in Table IV.

(Table IV). The presence of this wild-type signal suggests that His-200 is most likely not a copper-binding ligand in TfdA. As found for H113A and MBP-H167A, addition of α-KG and/or 2,4-D has little effect on the spectrum.

ESEEM Spectroscopic Characterization of Variants with Altered Metal Sites—Pulsed EPR (ESEEM) spectroscopy has

TABLE IV
Summary of the EPR spectral parameters for Cu(II)-substituted TfdA variants

	$g_\parallel$	$A_\parallel$	$g_\perp$
		mT	
Wild-type TfdA	2.34	16.3	2.07
Wild-type TfdA/α-KG	2.36	15.1	2.07
Wild-type TfdA/α-KG/2,4-D	2.38	12.0	2.09
H113A	2.30	16.6	2.07
H113A/α-KG	2.33	15.8	2.07
H113A/α-KG/2,4-D	2.35	14.0	2.08
D115A	2.30	17.0	2.06
D115A/α-KG	2.30	16.2	2.06
	2.34	16.8	2.06
D115A/α-KG/2,4-D	2.30	16.2	2.06
	2.34	16.8	2.06
MBP-H167A	2.30	17.1	2.07
MBP-H167A/α-KG/2,4-D	2.30	17.1	2.07
MBP-H200A	2.30	17.1	2.07
	2.34	16.1	2.07
MBP-H200A/α-KG/2,4-D	2.30	17.1	2.07
	2.34	16.1	2.07

per in a site with two histidyl residues directly coordinated to the metal. As previously reported (23), three-pulse ESEEM spectra collected in the $g_\parallel$ region for wild-type TfdA exhibit sharp peaks at 0.6, 0.9, and 1.5 MHz and a broad feature at 3.5 MHz (Fig. 3*B*). This signature is typical of imidazole bound in an equatorial position to copper. The additional appearance of narrow combination bands at 2.1, 2.5, and 3.1 MHz in these spectra indicated the presence of at least two such imidazole ligands bound to the copper (34–36). Spectral simulations using the density matrix approach of Mims (28) were used to analyze these data further including determination of the number of histidyl ligands coordinated to copper. The $g_\parallel$ ESEEM of Cu(II)-substituted wild-type TfdA was simulated with magnetic parameters for copper equatorially coordinated to two identical histidines with a simulation program using the angle selection scheme developed for ENDOR analysis (37, 38). For each simulation, a background decay function was applied to allow the amplitudes of the initial 1.5 μs of the simulations to match the data. The resulting simulated data sets (*dashed curves*) are superimposed on the experimental data in Fig. 3. Further analysis of these data suggested that formation of the ternary complex with α-KG and 2,4-D results in the probable loss or reorientation of one of these imidazole ligands, as evidenced by a substantial decrease in the modulation intensity and disappearance of the combination bands (23).

Three-pulse ESEEM patterns for the H113A (*trace A*), MBP-H167A (*trace B*), and D115A (*trace C*) variants of TfdA are shown in Fig. 4. Each data set was collected under identical conditions and normalized so that the integrated echo amplitudes range from zero, determined by shifting the integration window off of the signal at the end of a scan, to one which marks the largest measured echo amplitude. Low frequency modulations indicative of equatorially bound histidyl ligand(s) are observed for all four mutant TfdAs. The ESEEM from H113A (*trace A*) and MBP-H200A (not shown) variants are nearly identical and show modulations that are considerably weaker than those measured for MBP-H167A (*trace B*) and D115A (*trace C*). Each of these data contains a large unmodulated or DC component (well over 80% of the total signal intensity in the case of H113A), contrasting sharply with the ESEEM for copper-substituted wild-type TfdA, where the DC component constituted less than 40% of the total signal inten-

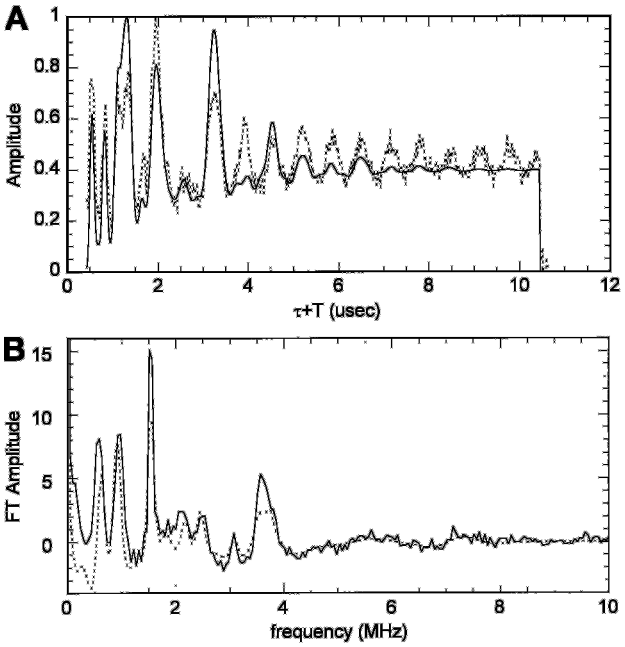

FIG. 3. **Three-pulse ESEEM spectrum and Fourier transformation of Cu(II)-substituted wild-type TfdA with 2-histidine simulation data.** ESEEM spectrum of wild-type Cu(II)-TfdA + α-KG (*solid*) and computer-simulated data for Cu(II) bound by two identical histidines (*dashed*) (*A*) and the corresponding frequency domain spectrum (*B*). Parameters for data collections were magnetic field = 2800 G, τ = 375 ns, T = 50 ns, ν = 8.98 GHz; 4.2 K. Cu(II) hyperfine parameters: g_{xy} = 2.05, g_z = 2.34, $A_{xx} = A_{yy}$ = 20 MHz, A_{zz} = 487 MHz; Superhyperfine parameters: g_N = 0.40347, A_{iso} = 1.7 MHz, radius = 2.75 Å [θ,ϕ] = [2.37,2.07] radians, e^2qQ = 1.60 MHz, η = 0.75, NQI [α,β,γ] = [0.50,1.1,0.1] radians. The simulated data were treated with an exponential decay function to give $y_{ij} = (y_{ij} - 0.17)\cdot\exp((\tau + T)/3500)^{1.5}) + 0.17$. For each simulation, a background decay function was applied to allow the amplitudes of the initial 1.5 μs of the simulations to match the data.

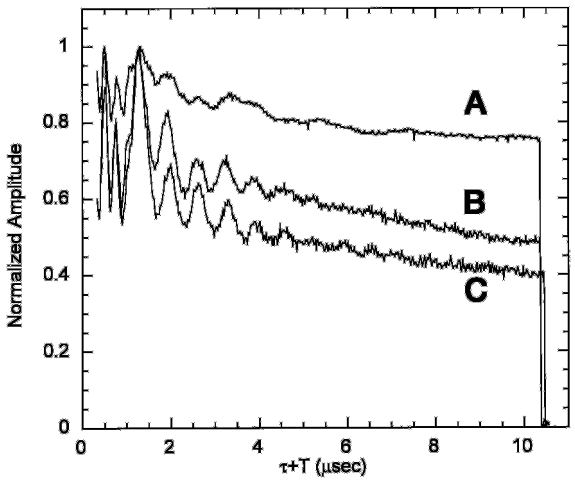

FIG. 4. **Three-pulse ESEEM time domain spectra of TfdA variants.** H113A Cu-TfdA (*A*), magnetic field = 3050 G, τ = 300 ns, T = 40 ns. MBP-H167A Cu-TfdA (*B*), magnetic field = 3100 G, τ = 300 ns, T = 40 ns. D115A Cu-TfdA (*C*), magnetic field = 3050 G, τ = 385 ns, T = 55 ns, ν = 8.8 GHz; 4.2 K.

features at 0.7, 1.5, and 4.0 MHz that are indicative of histidyl imidazole equatorially coordinated to Cu(II) (36). The spectra obtained for D115A and MBP-H167A variants are shown in Figs. 5*B* and 6*B* (*solid lines*), respectively. The resolution in these spectra is poor when compared with similar data ob-

DOCKET ALARM

Explore Litigation Insights

Docket Alarm provides insights to develop a more informed litigation strategy and the peace of mind of knowing you're on top of things.

Real-Time Litigation Alerts

Keep your litigation team up-to-date with **real-time alerts** and advanced team management tools built for the enterprise, all while greatly reducing PACER spend.

Our comprehensive service means we can handle Federal, State, and Administrative courts across the country.

Advanced Docket Research

With over 230 million records, Docket Alarm's cloud-native docket research platform finds what other services can't. Coverage includes Federal, State, plus PTAB, TTAB, ITC and NLRB decisions, all in one place.

Identify arguments that have been successful in the past with full text, pinpoint searching. Link to case law cited within any court document via Fastcase.

Analytics At Your Fingertips

Learn what happened the last time a particular judge, opposing counsel or company faced cases similar to yours.

Advanced out-of-the-box PTAB and TTAB analytics are always at your fingertips.

API

Docket Alarm offers a powerful API (application programming interface) to developers that want to integrate case filings into their apps.

LAW FIRMS
Build custom dashboards for your attorneys and clients with live data direct from the court.

Automate many repetitive legal tasks like conflict checks, document management, and marketing.

FINANCIAL INSTITUTIONS
Litigation and bankruptcy checks for companies and debtors.

E-DISCOVERY AND LEGAL VENDORS
Sync your system to PACER to automate legal marketing.